2023-01-0213

Multi-Plane PIV using Depth of Field for In-cylinder Flow Measurements

Christopher Willman, Qichi He, Benjamin A. O. Williams and Richard Stone
University of Oxford

Matthew McAllister
Jaguar Land Rover Limited

Abstract

Extending the planar Particle Image Velocimetry (PIV) technique to enable measurements on multiple planes simultaneously allows for some of the 3 dimensional nature of unsteady flow fields to be investigated. This requires less hardware and retains the typically higher spatial resolution of planar PIV compared to fully 3-dimensional PIV techniques. Performing multi-plane PIV measurements requires the light scattered from the different measurement planes to be distinguishable. This may be achieved by using different laser wavelengths which adds significantly to the expense and complexity of the system, by using different light sheet polarisations which is challenging for engine measurements through windows due to stress-induced birefringence, or by making alternating measurements of each plane which sacrifices the simultaneity of the flow measurement across multiple planes. In this work, simultaneous PIV measurements on two parallel offset planes are performed by modifying a standard two-dimensional two-component (2D2C) PIV system consisting of a single high-speed camera and a dual-cavity PIV laser. Image splitting optics with a variable optical path length were used to image two measurement planes onto the single camera sensor. The degree of defocus of the droplet images arising from the narrow depth of field was used to distinguish between the measurement planes. The robustness of the degree of defocus method for plane discrimination was evaluated using both representative test targets and experimentally obtained PIV images of the in-cylinder flow field of a spark ignition internal combustion engine (ICE). This depth of field based method enables simultaneous multi-plane PIV measurements of in-cylinder flows to be performed with only minor alterations to a standard 2D2C PIV system using off-the-shelf optics.

Introduction

Motivation for Multi-plane PIV measurements

Time-resolved volumetric velocity measurement techniques such as tomographic PIV [1], [2] or particle tracking velocimetry [3] enable investigation of unsteady 3-dimensional flows in practical thermofluid systems. However, acquiring volumetric information requires compromise to minimize overlapping particle images and enable accurate reconstruction of the volumetric spatial information. Typical approaches include using lower seeding densities (leading to lower spatial resolution) than equivalent planar techniques and restriction of the illuminated volume to a thick sheet (common width/height-to-depth aspect ratios are around 4:1) [4], [5]. The 3D reconstruction process for tomographic PIV using limited views can also lead to increased errors in derived flow parameters compared to planar techniques [4].

For simultaneous measurement of velocity fields on two or more offset planes within a flow, in some cases planar techniques can be preferable to volumetric techniques, particularly if the offset between the planes is large or high spatial resolution within the planes is required. In order to perform two or more simultaneous planar measurements, light originating from each plane must be distinguishable.

Plane discrimination in Dual/Multi-plane PIV

Dual-plane PIV typically refers to extracting local 3D properties of the flow (e.g. vorticity) from two closely spaced planes [6], although it has also been used to refer to performing two PIV measurements on well-separated planes [7]. For clarity, this work uses “multi-plane PIV” to describe performing PIV measurements on two or more distinct planes with the aim of characterising large scale or spatially separated flow features.

Discriminating the scattered light originating from each of the two planes of dual-plane PIV may be achieved via polarization [8], wavelength [9] or temporal separation [7], and the concepts may be applied to multi-plane PIV with larger plane separations and also combined to increase the number of measurement planes [10], [11].

Polarization based dual-plane PIV cannot be trivially extended to more than two planes and is challenging to apply to enclosed flows with birefringent windows. Use of multiple laser wavelengths can conceptually scale to simultaneous measurements on many offset planes, at the expense of additional laser systems or wavelength-shifting optics. Alternating PIV measurements on each plane at different times prevents cross-talk from the out-of-focus plane and the concept can be extended to more than two planes by sequentially scanning the laser sheet across multiple depths [12]. However, this technique can only make quasi-simultaneous measurements if the flow behaviour is 'slow' on the timescale of scanning or if sequential measurements on a given plane are interpolated in time.

In this work, novel simultaneous multi-plane PIV measurements are performed within the enclosed flow of an optically accessible internal combustion engine using the degree of defocus in the droplet images to discriminate between the two measurement planes. This technique enables multi-plane PIV to be performed with a standard 2D2C single-camera PIV system via the addition of image splitting optics. The approach does not suffer from stress-induced birefringence of the optical access windows and has the potential to be combined with existing methods for plane separation (e.g. wavelength) to further increase the number of available measurement planes.

Depth from defocus in microscopy

The encoding of depth information in the characteristics of defocused images has been extensively studied in microscopic particle image velocimetry (μPIV).

In μPIV, the thickness of the measurement volume is often defined by the depth resolution of the imaging system, rather than the

thickness of the light sheet, due to the difficulty in selectively illuminating sub-mm structures (e.g. in microfluidic devices) with a light sheet. Various methods have been developed to quantify the characteristics of images arising from particles at different depths to improve spatial resolution and to enable volumetric measurements.

Numerical approaches either leverage the depth-dependence of the size of blurred particle images i.e. “depth from defocus” [13], [14], or compare characteristics of the defocused particle images to calibrated images at known depths as implemented in General Defocusing Particle Tracking (GDPT) [15], [16].

Optical approaches involve adding optical elements to the imaging system. Addition of a multi-aperture mask within the imaging system creates multiple copies of each particle image on the camera sensor, with the spacing of the duplicated images varying as a function of the particle’s depth within the measurement region [17]–[20]. This relies on identification of individual particle images at much lower particles-per-pixel seeding densities than typical macroscopic PIV. Adding a cylindrical lens or modifying existing optics to introduce astigmatism causes a depth-dependent variation in the shape of the particle images [21], [22]. A distorted diffraction grating may be designed to give a different focusing power for different diffraction orders, altering the effective power of the imaging system to form images from different depths at laterally displaced positions on the camera sensor [23], [24].

In multifocal plane microscopy, the imaging path is split into arms with differing optical path lengths after the objective lens in order to form in-focus images from different depths within the sample for each path [25], [26]. Practical extensions to this technique include the use of a Z-splitter prism to image multiple planes of differing depths simultaneously onto a single camera sensor [27].

The optical arrangement for depth-of-field-based plane discrimination proposed in this work is a macroscopic extension of this Z-splitter prism technique. Scattered light from the measurement planes is imaged via two optical paths of different length onto a single camera sensor. The remaining challenge is then to accurately calculate PIV vector fields from images which contain both in-focus desired particle images and out-of-focus undesired particle images.

Multi-plane PIV plane discrimination via depth of field

In µPIV, the “depth of correlation” is used to quantify the range of depths over which µPIV tracer particles contribute to the cross-correlation and therefore the derived vector field. This parameter may be calculated by considering geometric optics, diffraction and particle size [5], however experimentally measured values are in some cases larger by an order of magnitude which may be accounted for by application of correction factors [28].

The larger scales involved in multi-plane PIV permit selective illumination of only the two (or more) planes of interest, instead of the effectively volume-illumination common in µPIV. This means that for macroscopic multi-plane PIV there are only discrete classes of out-of-focus droplet images to consider, rather than a continuous range of defocused image characteristics. This simplifies the analysis as the depth information of the two planes is known, only requiring discrimination of signals from each plane for which detailed numerical methods such as GDPT are not required.

Using a standard imaging arrangement forms one image of the measurement region on the camera sensor, with contributions from all illuminated planes at once. These contributions may be discriminated by a numerical segmentation algorithm to classify each particle image based on the size and intensity of the defocused images, a procedure that becomes challenging at high seeding densities [29].

In this work, image splitting optics with a variable optical path length allow a single camera to image two parallel offset planes with each plane in focus in only one of the two copies of the image on the camera sensor. Images from the out-of-focus plane are blurred and spread their intensity over a greater number of pixels, contributing less to the intensity-dependent cross-correlation calculations in the PIV processing routine. Ideally a narrow depth of field causes the out-of-focus plane images to blur to form a near-uniform background, enabling unbiased PIV measurements on the in-focus plane.

In practice, scattered light from each PIV seeding droplet within the out-of-focus plane forms its own blurry image on the camera sensor, with a size and spatial intensity distribution characteristic of both the displacement (distance and direction) of the droplet from the object plane and the aberrations present in the imaging system. Variations in seeding density will affect the number density and degree of overlap of the blurry images, but not the characteristic features of each out-of-focus droplet image.

These blurry images move between frames due to the motion of the flow on their plane of origin. Any contribution they make to the cross-correlation introduces the potential for the PIV algorithm selecting the “wrong” correlation peak or biasing the location of the “correct” correlation peak. Contributions to the correlation function vary with intensity squared [5]. Successful discrimination of planes via the blurring of out-of-focus images relies on spreading out the light scattered from each droplet in the out-of-focus plane over a larger area to reduce the peak intensity.

Paper structure

This paper demonstrates a proof-of-principle that a single camera 2D2C PIV system may be modified with off-the-shelf optics to perform simultaneous multi-plane PIV measurements in a practical thermofluid system. This is achieved by leveraging a narrow depth of field and image splitting optics with a variable optical path length to discriminate between measurement planes at different depths.

Two experimental setups were used to validate the depth of field method for multi-plane PIV. Firstly, translation of static representative PIV targets is used to provide a known displacement with which to evaluate the robustness of multi-plane PIV calculations as a function of plane separation.

Secondly, an optically accessible internal combustion engine is seeded with oil droplets and motored to compare velocity fields derived from the multi-plane PIV technique to those derived from conventional single-plane PIV measurements. Due to the cyclic variability of the in-cylinder flow field, comparisons are restricted to mean flow fields.

Experimental apparatus and procedure

Image splitting optics with variable optical path

The multi-plane PIV technique of this work performs measurements on two parallel offset planes “A” and “B” with a separation of Δx. [Figure 1]. To enable images from the two offset planes to be brought into focus on a single camera sensor, an image splitting arrangement

based on a 50/50 beamsplitter (Thorlabs BSW42-532) and enhanced aluminium coated prism mirrors (Edmund Optics 49-406) was constructed. Elastically-scattered light from both planes travels along both legs of the image splitting arrangement. The optical path length in each leg can be adjusted to form an in-focus image of either plane A or plane B on the camera sensor. This condition is shown in Figure 1, where planes "A" and "B" have been coloured green and blue respectively, to match the mirrors in their corresponding "in-focus" leg. Translation stages allow for the optical path in each leg to be independently varied by up to ± 50 mm from their reference path length. In this work, the reference position was set to provide equal optical path lengths for the beamsplitter-transmitted path [Figure 1, green] and the beamsplitter-reflected path [Figure 1, blue]. A large diameter camera lens (f = 85 mm, f/1.2) images the object planes A and B onto a high-speed PIV camera (Phantom VEO 710L).

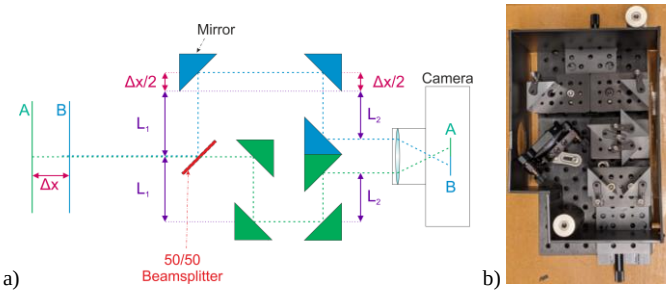

Figure 1 Image splitting optics with variable optical path. a) Diagram of optical paths which form in-focus images of the object planes "A" and "B" on the camera sensor. (Object planes and mirrors are coloured green and blue to aid in identification of the two intended optical path lengths). b) Photo of assembled image splitting optics mounted on a 150 mm x 300 mm breadboard.

Laser sheet splitting optics

To generate two parallel laser sheets with variable separation by splitting the PIV laser output pulses, a 50/50 non-polarised beamsplitter (Edmund Optics 35959), a dielectric prism mirror (Edmund Optics 37654) and a pair of anti-reflection coated cylindrical lenses (f = – 50 mm, Edmund Optics 37599) were mounted in a Thorlabs 30 mm cage system [Figure 2].

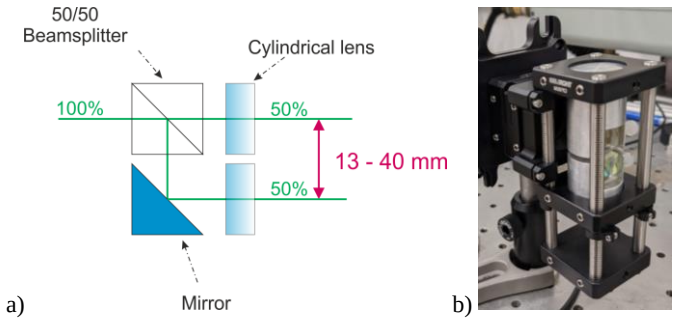

Figure 2 a) Diagram of twin sheet generation optics with variable plane separation. The axes of the cylindrical lenses are vertical in this figure, producing two parallel sheets which diverge in a horizontal plane. b) Photo of assembled twin sheet generation optics within a Thorlabs 30 mm cage system.

Representative PIV targets

Representative PIV targets were prepared to evaluate the robustness of the proposed degree of defocus method for discriminating measurement planes. Tracer particles (Polyamide Seeding Particles, diameter 5 µm, Dantec Dynamics) were distributed across the surface of two microscope slides (see Figure 3 for examples of the tracer particle images). Each slide was mounted on a pair of orthogonal translation stages, with controllable axial and lateral translations to provide a pair of parallel PIV target planes [Figure 4].

For each plane separation, set by axial translation of the stages, PIV measurements were simulated by illuminating the two target slides simultaneously with an LED and taking an image with a high-speed CMOS camera (Photron FASTCAM 1024PCI). The slides were then given opposite lateral translations (indicated by blue arrows in Figure 4), followed by a second image being taken. Each image pair therefore contains both in-focus and out-of-focus particle images, with the two classes of particle images showing opposing displacements between the camera images.

The Matlab package PIVlab (v2.56) was used to calculate an apparent velocity field from each image pair using an FFT based multi-pass cross-correlation routine [30]. The interrogation window size was reduced from 64x64 pixels to 32x32 pixels, with 50% overlap between each window.

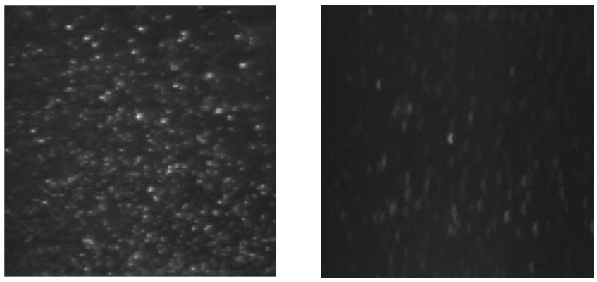

Figure 3 Example of tracer particles images: (a) in-focus; (b) out-of-focus with 15 mm plane separation from the in-focus plane.

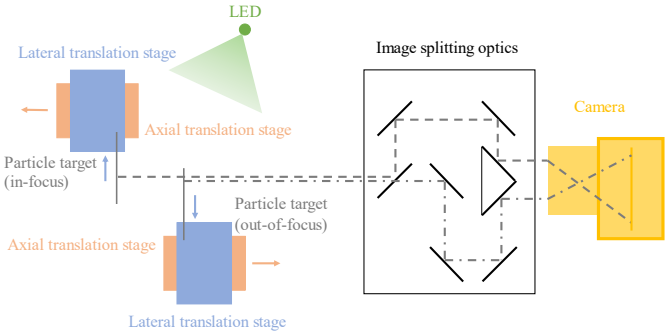

Figure 4 Particle target test setup diagram (not to scale).

Optical engine PIV measurements

The optical engine and PIV system used in this work have been described in detail previously [31]. A brief description is provided here for convenience.

Multi-plane PIV measurements were performed in a single cylinder, optically accessible GDI engine every 5°CA during the compression stroke from −120°CA to −55°CA aTDC. The engine was operated under motored conditions [Table 1]. A LaVision aerosol generator was used to seed olive oil droplets (approximately 0.2 – 0.4 µm diameter) into the intake plenum. A fused silica optical access annulus provided optical access for the PIV laser sheets (1 mm thick, approximately 30 mm wide) generated by a double cavity Nd:YLF

laser (Photonics Industries DM20-527-DH) operating at 527 nm, to illuminate two horizontal swirl planes. The upper plane was parallel to and 2.5 mm below the firing deck. The lower plane was displaced 15 mm below the upper plane. A Bowditch piston and 45° mirror arrangement enabled the swirl planes to be imaged through the piston crown window onto a high-speed CMOS camera (Phantom VEO 710L) [Figure 5].

Table 1 Engine specifications

Bore	85 mm
Stroke	90 mm
Valves per cylinder	2 intake, 2 exhaust
Engine speed	1000 rpm
Intake pressure	70 kPa
Intake air temperature	316 K
Coolant temperature	296 K
Intake air volume flow rate	1.65 Ls^{-1}

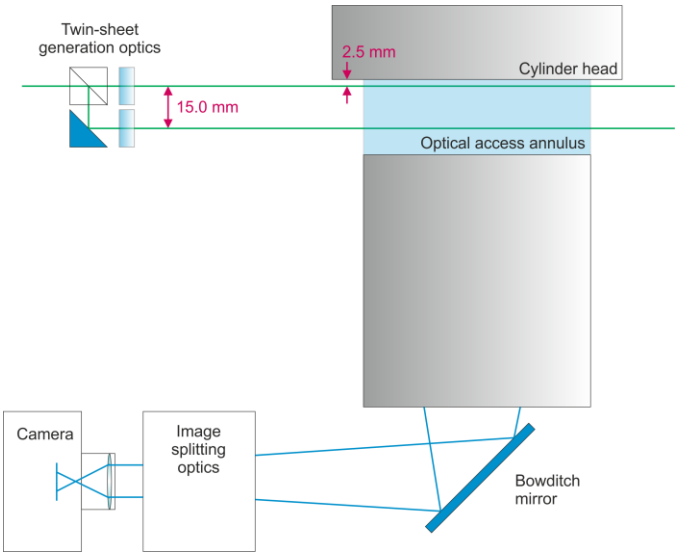

Figure 5 Geometry of the optical engine, sheet delivery and imaging system.

For a typical in-cylinder 2D2C PIV measurement, the time separation between laser pulses, "dt", is varied as a function of crank angle to achieve an optimal pixel shift of the droplet images. For the multi-plane PIV of this work, selection of "dt" values must consider both measurement planes as the laser sheets for each originate from the same pair of laser pulses. Additionally, the swirl plane measurements for flows with strong tumble motion can lead to significant out-of-plane motion at the inlet and exhaust sides of the measurement region. For some measurement timings, values of "dt" were reduced from the optimal quarter-window pixel shift to reduce droplet image pair losses due to out-of-plane motion.

All image acquisition and processing was performed using LaVision DaVis 8.4.0 software following the routine detailed in [31]. This routine was optimized for standard 2D2C PIV under similar conditions in the optical engine and includes a sliding average filter across cycles to remove scattered light from static sources, followed by a multi-pass cross-correlation algorithm with a final interrogation window size of 32×32 pixels. The resulting vector spacing is 2.17 mm due to the 50% overlap of the interrogation windows. Two regions of intense scatter from cylinder head features were masked during the image pre-processing, leading to the two regions without vectors near x = 20 mm and x = −20 mm for Figure 11 onwards. As a 2D2C technique, unless otherwise stated all discussion of velocity directions and magnitudes refers to in-plane velocity only. Of note is that this is a "typical" single-plane PIV processing routine: no attempt was made to identify or reduce the contribution of out-of-focus droplet images to the cross-correlation calculations by numerical methods.

Results

Representative PIV targets

Figure 6 and Figure 7 show the apparent velocities calculated from the known translation of the particle-covered slide test targets detailed in Figure 4. For conciseness, only data derived from the images obtained via the beamsplitter-reflected path [Figure 1, blue] are shown. For each plane separation, 86 vectors across the field of view are analysed.

A preliminary in-focus single-plane measurement provides a nominally correct result for comparison to the multi-plane data. This single-plane measurement is recorded with the out-of-focus slide removed and is used to normalise the apparent velocities of the multi-plane data, so that a value of "1" represents an exact match to the single-plane data. A normalised apparent velocity of "−1" represents a velocity vector in the opposite direction to this reference case (i.e. in the direction of the out-of-focus slide motion). The deviation of the apparent velocities from the reference case in Figure 6 and Figure 7 indicates the extent of the cross-talk between the two measurement planes as a function of plane separation.

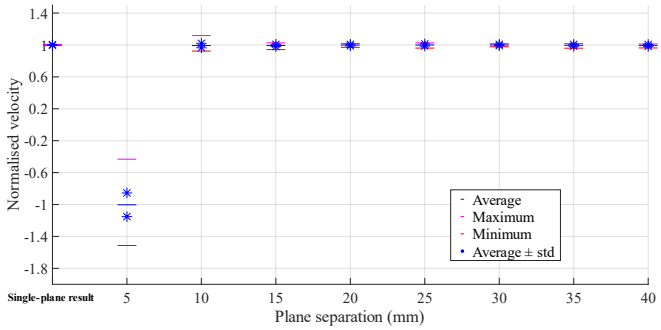

Figure 6 Measurement of the apparent velocity of the in-focus particle-covered slide test target as a function of plane separation. The in-focus and out-of-focus test targets of Figure 4 were given known opposed translations between images 1 and 2 of each PIV image pair. A nominally correct in-focus single-target PIV measurement is plotted at 0 mm for reference.

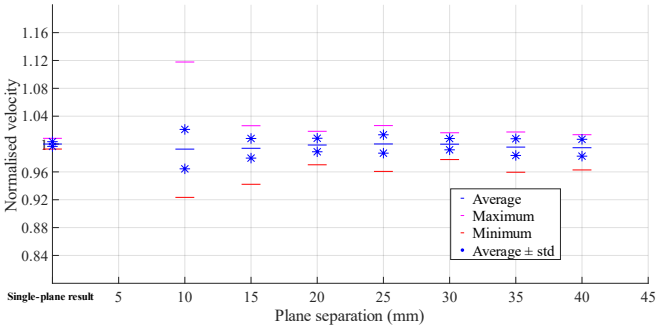

Figure 7 A copy of Figure 6 with an enlarged velocity scale to highlight differences between results for plane separations ≥ 10 mm.

It is observed that the PIV cross-correlation algorithm cannot successfully recover the apparent velocity of the in-focus particle

slide for a plane separation of 5 mm. At a plane separation of 10 mm, the mean normalised velocity (± one standard deviation) of the 86 vectors is 0.993 ± 0.028, compared to the ideal result of "1". For plane separations ≥ 15 mm, the mean normalised velocities are all within 0.6% of "1" with standard deviations smaller than 1.5%.

Optical engine

In this section, results from multi-plane PIV measurements of the flow field in a motored optically accessible engine are presented and evaluated.

Plane separation selection

Evaluation of the multi-plane PIV method using in-cylinder flows was undertaken with a plane separation of 15 mm. Under the approximately equivalent optical conditions of the particle slide tests, 15 mm was the minimum plane separation for which the 86 vectors achieved: an average error of ≤0.6%, a standard deviation of <1.5% and individual derived velocities all within 6% of the correct value. Future work will investigate the effect of plane separation in more detail, but in this work 15 mm may be assumed to be the most challenging (smallest) separation of planes within the recommended range of ≥ 15 mm established in the particle slide tests. A plane separation of 15 mm also enables a conveniently compact design for the generation of parallel laser sheets from a single beam path using off-the-shelf 12.5 mm optics [Figure 2]. The upper plane is at a height of 2.5 mm below the firing deck (selected as the highest possible plane at which a laser sheet could be introduced through the optical annulus), while the lower plane is 15 mm below the upper plane.

Test condition selection

Previous work with the optical engine shows a dominant tumble motion with an axis of rotation approximately parallel to the crankshaft [31]. As the piston rises during the compression stroke, the tumble vortex centre rises through the lower plane. This enables three distinct flow conditions on the pair of swirl planes to be investigated with suitable selection of measurement timings.

- **Similar flows with slight differences in direction and magnitude:** At −110°CA aTDC, the tumble vortex centre lies below the lower measurement plane and the dominant motion on both measurement planes is inlet-to-exhaust flow.
- **One stable, high velocity flow and one highly variable flow with regions of low velocity:** At −75°CA aTDC, the tumble vortex centre lies within the lower measurement plane. The upper plane retains the dominant inlet-to-exhaust flow, while the flow on the lower plane is highly variable in direction and gives lower mean in-plane velocities.
- **Opposed flows:** At −60°CA aTDC, the tumble vortex centre lies between the lower and upper measurement planes. The flow either side of the tumble vortex centre gives an inlet-to-exhaust flow for the upper plane and an exhaust-to-inlet flow for the lower plane.

Example multi-plane PIV images

Figure 8 shows an example single-frame image recorded by the high-speed PIV camera with both the upper and lower planes illuminated by the laser sheets. The images arising from the "upper" and "lower" planes are superimposed on the camera sensor with an offset specified by the final stage of the image splitting optics (approximately 35 mm in object-space). Before PIV processing, this dual image is separated and calibrated to give one "upper" image and one "lower" image. The exhaust and inlet sides of the engine are labelled in Figure 8, this view orientation is maintained throughout the PIV vector fields in this paper.

In both the upper and lower images of Figure 8, scattered laser light from droplets in both planes reaches the camera sensor, producing two classes of droplet images: in-focus and out-of-focus. To isolate the contribution from droplets on the upper plane, Figure 9 shows an example single-frame image recorded with only the upper laser sheet active.

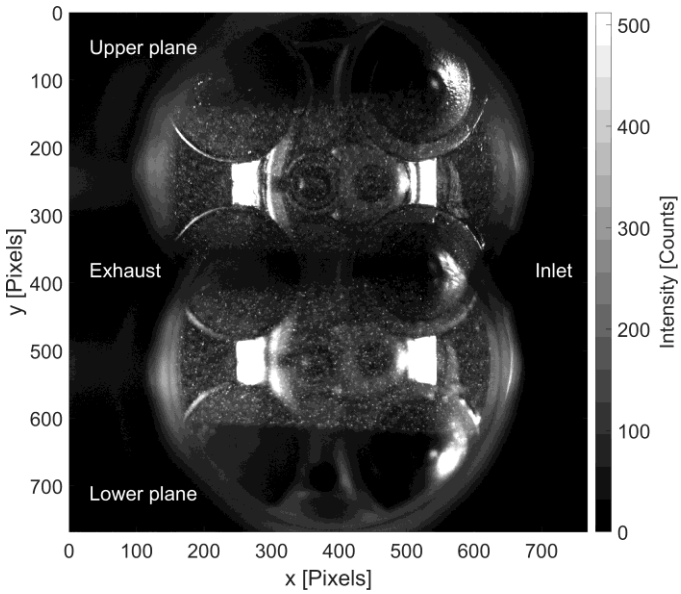

Figure 8 Example in-cylinder multi-plane PIV image with both planes illuminated.

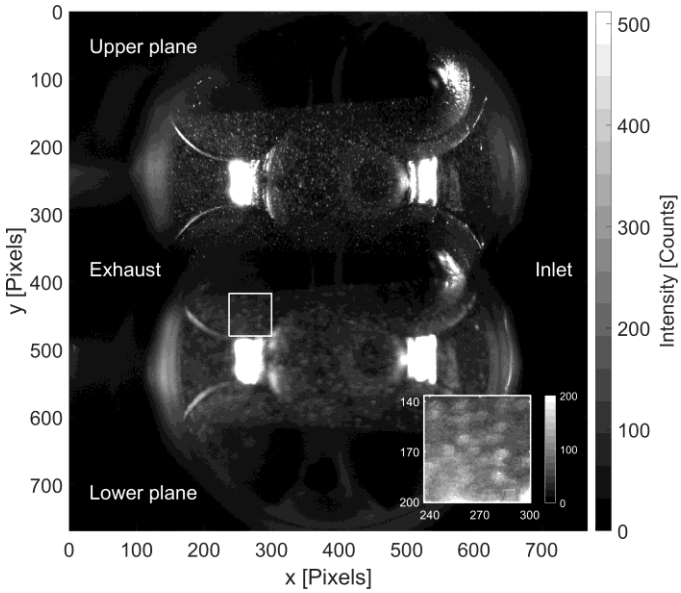

Figure 9 Example in-cylinder multi-plane PIV image with only the upper plane illuminated. Inset figure highlights the detail of out-of-focus droplet images within the region bounded by the white rectangle near co-ordinates (x,y) = (250,450).

The upper plane image contains only in-focus droplet images, effectively a standard 2D2C PIV image. The degree of defocusing at this plane separation can be observed in the lower plane image: light

scattered from upper plane droplets forms diffuse out-of-focus droplet images on the lower plane image. Detail of the intensity pattern produced is shown in the inset figure, with light from each droplet spread over a diameter of approximately 8 pixels, with a corresponding reduction in peak intensity value compared to the in-focus droplet images.

Figure 10 shows an equivalent example image with only the lower laser sheet active. In contrast to Figure 9, the out-of-focus droplet images of the upper plane image have a distinct sharp-edged character, with intensity concentrated at the edges of each circular blurred image. This asymmetric behaviour of out-of-focus images from objects in front vs behind the plane of best focus (foreground vs background bokeh) is consistent with an imaging system with under-corrected spherical aberration.

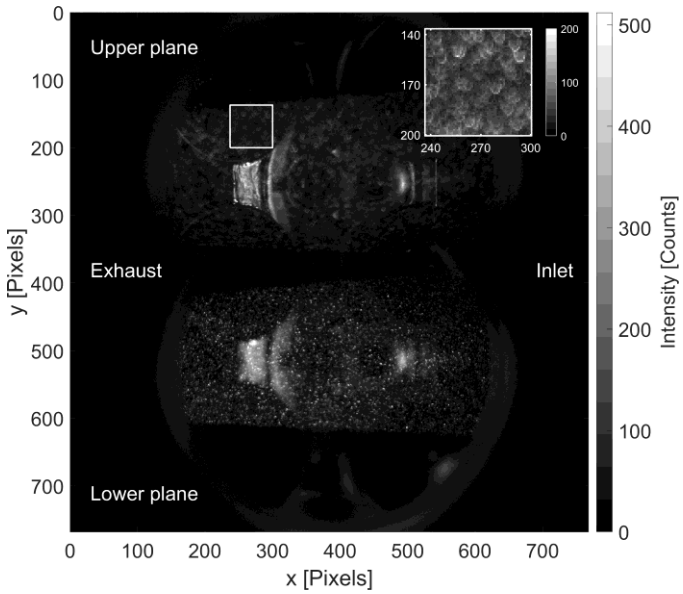

Figure 10 Example in-cylinder multi-plane PIV image with only the lower plane illuminated. Inset figure highlights the detail of out-of-focus droplet images within the region bounded by the white rectangle near co-ordinates (x,y) = (250,150).

The diffuse character of the background bokeh [Figure 9] is desirable for the out-of-focus images as it reduces the peak intensities and results in a more homogeneous intensity pattern, competing less effectively with the in-focus droplet image contributions to the cross-correlation of the PIV processing. The sharper character of the foreground bokeh [Figure 10] is more problematic, retaining smaller-scale, higher intensity patterns despite being nominally out-of-focus.

This leads to two competing influences on the selection of camera lens aperture. A narrow depth of field is beneficial for this multi-plane PIV technique, implying a fully open camera lens aperture of *f*/1.2. Aberrations are typically strongest towards the edges of a lens and reducing the contribution of wide-angle rays by reducing the camera lens aperture softens the sharp edges of the foreground bokeh.

The images in this work were recorded with an aperture of *f*/2 (reduced from the maximum of *f*/1.2) to partially soften the sharp edges of the foreground bokeh at the expense of a factor of 2.8 in light-gathering. In future work, a camera lens with variable spherical aberration control (e.g. Nikon AF DC-NIKKOR 105mm *f*/2 D) would provide an alternative mechanism for optimizing the blur characteristics.

Cross-talk from out-of-focus plane

The potential for cross-talk between measurement planes may be evaluated by applying the PIV processing routine to datasets with only the upper [Figure 9] or lower [Figure 10] laser sheet illuminating the in-cylinder flow.

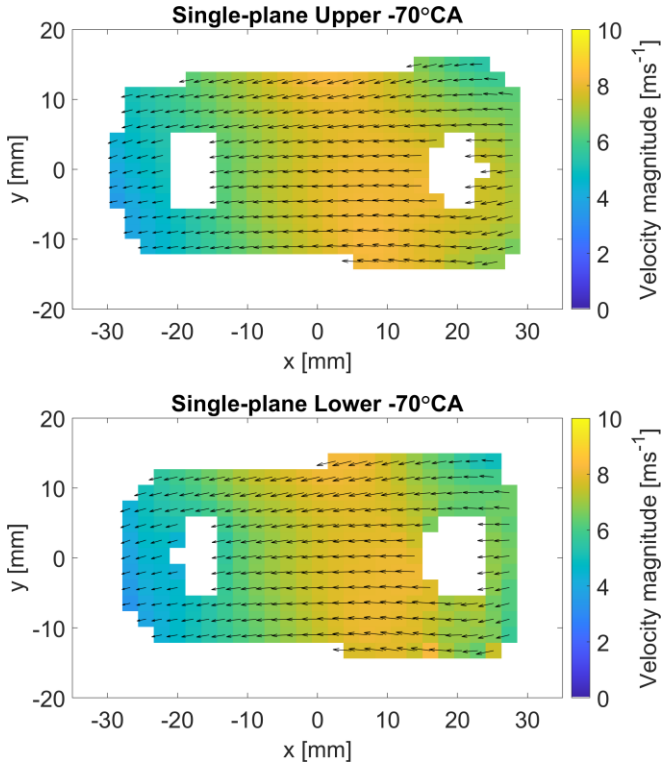

Figure 11 500-cycle mean velocity fields at −70°CA aTDC calculated using only upper sheet illumination [Figure 9].

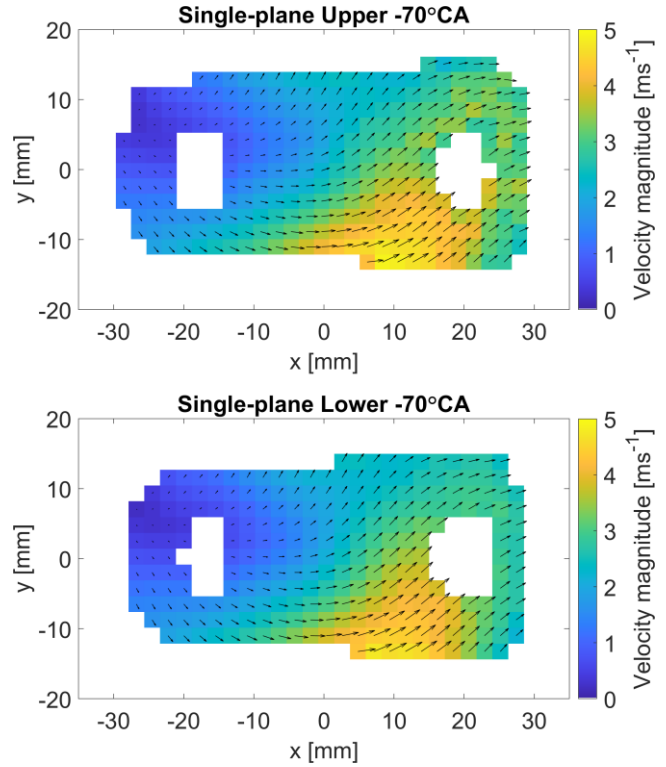

Figure 12 500-cycle mean velocity fields at −70°CA aTDC calculated using only lower sheet illumination [Figure 10].

The resulting mean vector fields, averaged over 500 cycles, show that the information content of the out-of-focus droplet images is sufficient to approximate the in-focus vector field for single-plane illumination with either the upper laser sheet only [Figure 11] or the lower laser sheet only [Figure 12]. Successful discrimination of the flow fields in each plane for multi-plane PIV measurements must therefore rely on the in-focus "correct plane" contribution to the cross correlation dominating the out-of-focus "other plane" contribution.

Multi-plane PIV vector fields

The cyclic variability of the in-cylinder flow field prevents knowledge of the "true" vector field for comparison to any individual multi-plane PIV measurement. Accordingly, 500-cycle mean flow fields were obtained with single-plane illumination in sequential experiments to provide nominally "correct" vector fields for comparison to 500-cycle multi-plane PIV mean flow fields obtained simultaneously on both planes.

Figure 13, Figure 14 and Figure 15 compare the multi-plane and single-plane 500-cycle mean flow fields for the three measurement timings identified previously to provide flows across the two planes which are similar (−110°CA aTDC), differing in velocity magnitude and directional stability (−75°CA aTDC) and opposed (−60°CA aTDC) (see: *test condition selection*).

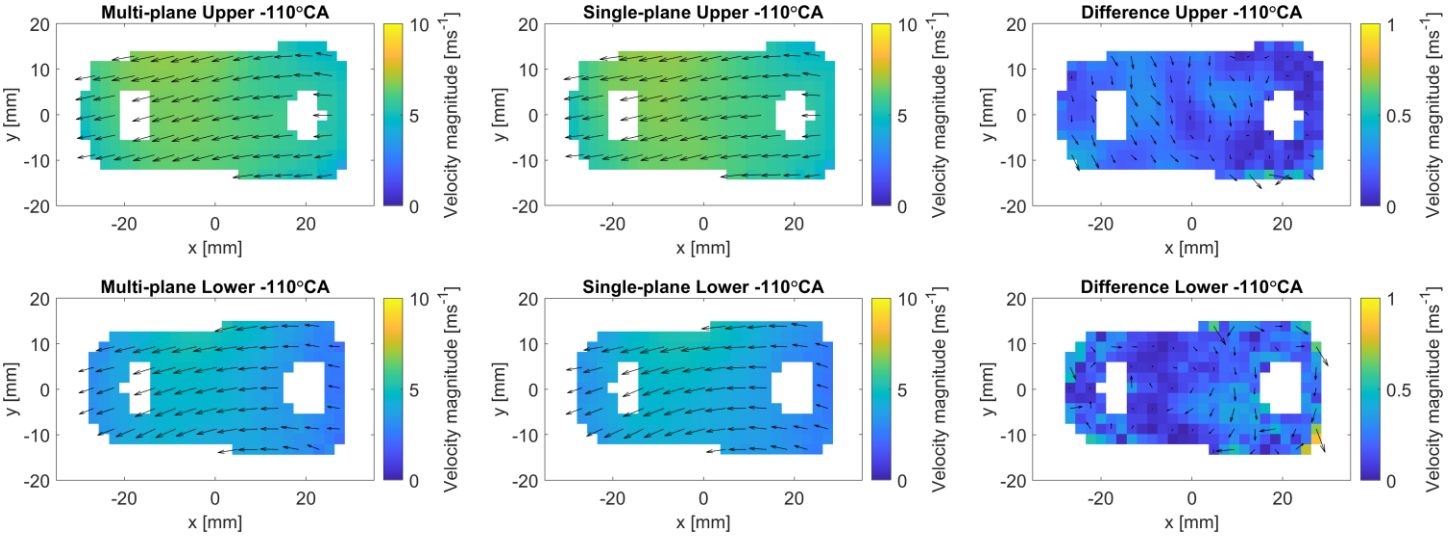

Figure 13 Left: Multi-plane PIV mean flow fields calculated from 500 cycles of simultaneous PIV measurements with both-sheets-illuminated. Centre: Single-plane PIV mean flow fields calculated from two non-simultaneous sets of 500 cycles of PIV measurements with only the upper or lower sheet illuminated. Right: Difference between Multi-plane and Single-plane mean vector fields. In each dimension, only 1 in 2 vectors have been plotted for clarity. At −110°CA aTDC, the tumble vortex centre lies below the lower measurement plane and the dominant motion on both measurement planes is inlet-to-exhaust flow, leading to similar flows on both planes with slight differences in direction and magnitude

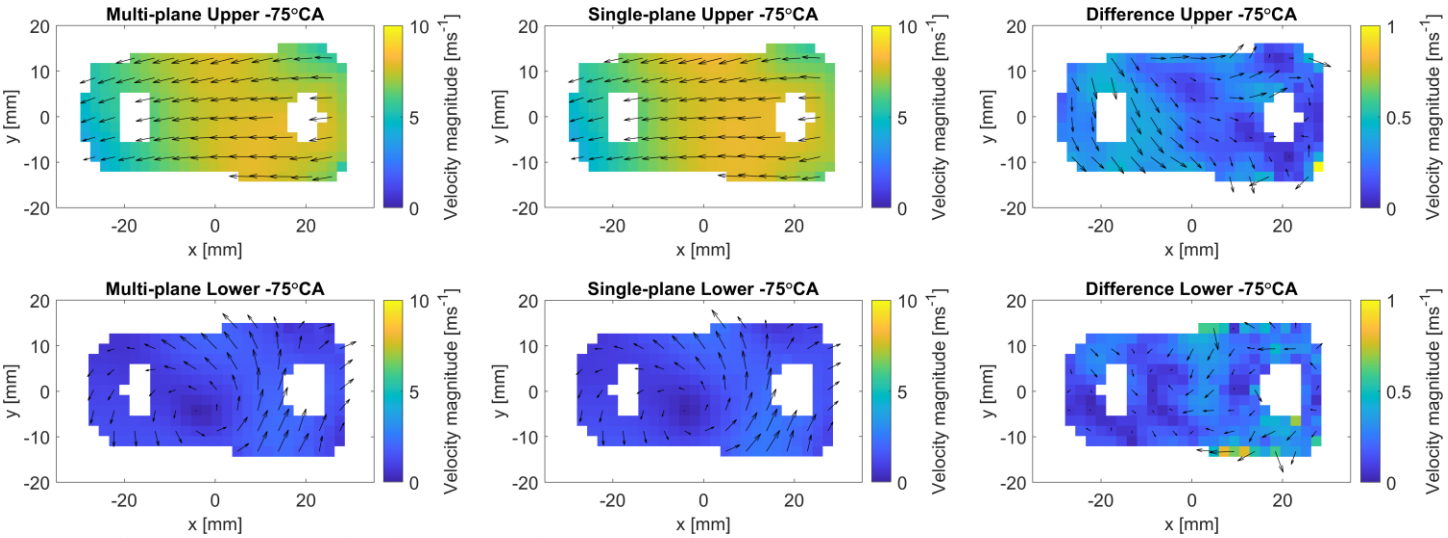

Figure 14 Left: Multi-plane PIV mean flow fields calculated from 500 cycles of simultaneous PIV measurements with both-sheets-illuminated. Centre: Single-plane PIV mean flow fields calculated from two non-simultaneous sets of 500 cycles of PIV measurements with only the upper or lower sheet illuminated. Right: Difference between Multi-plane and Single-plane mean vector fields. In each dimension, only 1 in 2 vectors have been plotted for clarity. At −75°CA aTDC, the tumble vortex centre lies within the lower measurement plane, leading to a stable, high velocity flow on the upper plane and a highly variable flow with regions of low velocity on the lower plane.

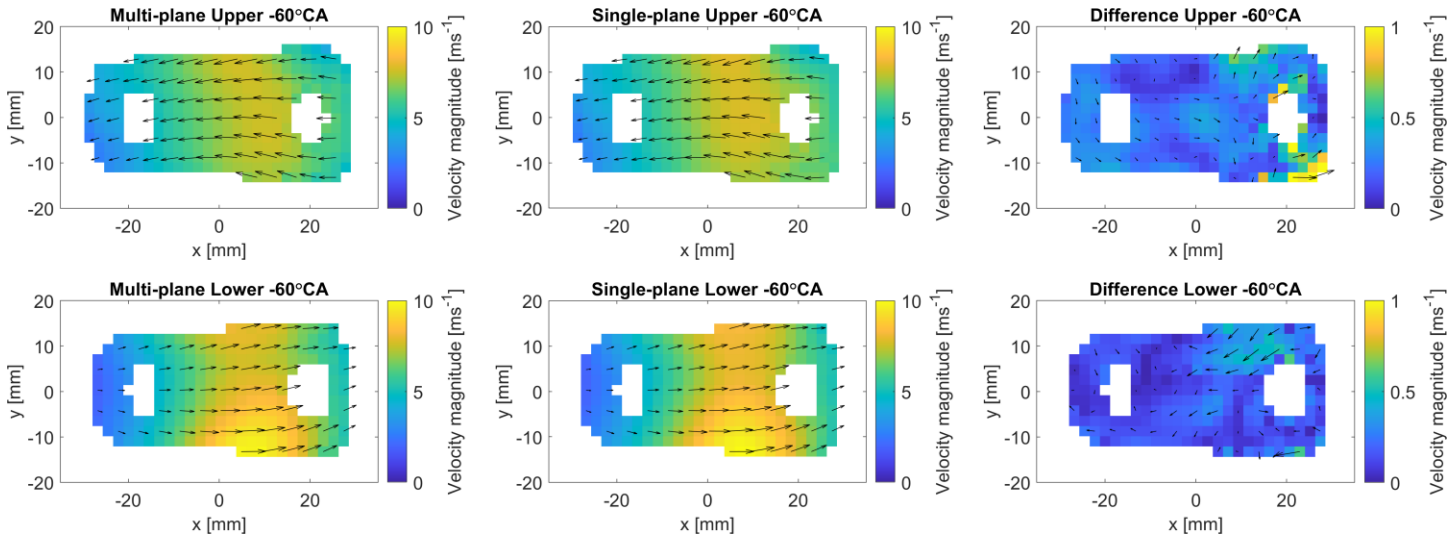

Figure 15 Left: Multi-plane PIV mean flow fields calculated from 500 cycles of simultaneous PIV measurements with both-sheets-illuminated. Centre: Single-plane PIV mean flow fields calculated from two non-simultaneous sets of 500 cycles of PIV measurements with only the upper or lower sheet illuminated. Right: Difference between Multi-plane and Single-plane mean vector fields. In each dimension, only 1 in 2 vectors have been plotted for clarity. At −60°CA aTDC, the tumble vortex centre lies between the lower and upper measurement planes, leading to opposed flows on the two planes.

Despite the potential for cross-talk highlighted in Figure 11 and Figure 12, the multi-plane PIV vector fields for all three flow conditions are sufficiently accurate to produce representative 500-cycle mean flow fields for two parallel offset planes, with mean velocities spanning 0 – 10 ms^{-1}. The differences between the multi-plane and single-plane PIV vectors are also displayed in Figure 13, Figure 14 and Figure 15, with a spatially-averaged difference of 0.21 ± 0.25 ms^{-1} for the lower plane and 0.25 ± 0.26 ms^{-1} for the upper plane across the three measurement timings (95% CI).

Notable discrepancies in the "difference" vector fields occur preferentially to the inlet side of the measurement region around x = 20 mm, at the edges of the masked region. Increased out-of-plane motion towards the inlet side coupled with reduced information within the PIV interrogation window at the edges of the masked region may have contributed to these increased differences.

These differences reflect the combination of cyclic variability in the flow field with the inherent uncertainties of the multi-plane PIV and single plane PIV techniques.

Cyclic variability comparison

In order to quantify the influence of cyclic variability in the flow field on the multi-plane PIV to single-plane PIV comparison, quantitative comparisons of flow fields from −120°CA to −55°CA aTDC were performed using the Relevance Index (RI) [32]. The RI is defined as

$$RI = \frac{\langle \overrightarrow{q_A}, \overrightarrow{q_B} \rangle}{\|\overrightarrow{q_A}\| \cdot \|\overrightarrow{q_B}\|} \qquad (1)$$

where $\langle \overrightarrow{q_A}, \overrightarrow{q_B} \rangle$ is the inner product between two vector fields $\overrightarrow{q_A}$ and $\overrightarrow{q_B}$, and $\|\vec{q}\|$ is the $\mathbb{L}^2$ norm of $\vec{q}$. RI values between two fields range from $+1$ for exact alignment to -1 for exactly opposite alignment.

For every measurement timing, the 500-cycle multi-plane and single-plane datasets were each split into two 250-cycle datasets and the RI was calculated between permutations of the 250-cycle datasets. Considering the single-plane to single-plane RI comparison as a baseline provides one measure of the cyclic variability of the in-cylinder flow field.

Figure 16 shows the RI values for the single-plane to single-plane flow field comparison on the upper plane (blue circles), which measures the differences between a pair of 250-cycle mean flow fields arising from cyclic variability of the in-cylinder flow field and uncertainty in the single-plane PIV technique. Defining a threshold RI value (full range −1 to 1) above which two flows may be considered "well-matched" is subjective, however threshold values of 0.95 to 0.99 are typical for in-cylinder flow literature [33]. Here the single-plane data provides a very good match to both the multi-plane data (mean RI = 0.9990) and the other 250-cycles of single plane data (mean RI = 0.9994). The comparison between each of the two 250-cycle mean multi-plane PIV flow fields produces a consistently poorer match (mean RI = 0.9975), albeit still a very good match overall.

A similar trend is displayed in Figure 17 for the lower plane flow fields. At −75°CA aTDC the tumble vortex centre lies within the lower plane. The resulting highly variable flow direction and low mean velocities cause a reduction in the similarity of sequential 250-cycle mean flow fields for all 3 RI comparisons.

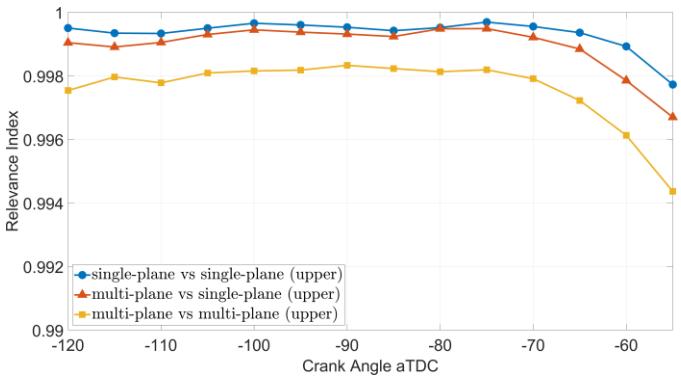

Figure 16 Relevance Index (RI) comparisons of the similarity of 250-cycle mean vector fields from the multi-plane and single-plane PIV techniques as a function of crank angle during the compression stroke for the upper plane. The 250-cycle datasets used for this comparison were obtained by splitting each of the 500-cycle multi-plane and single-plane datasets into two.

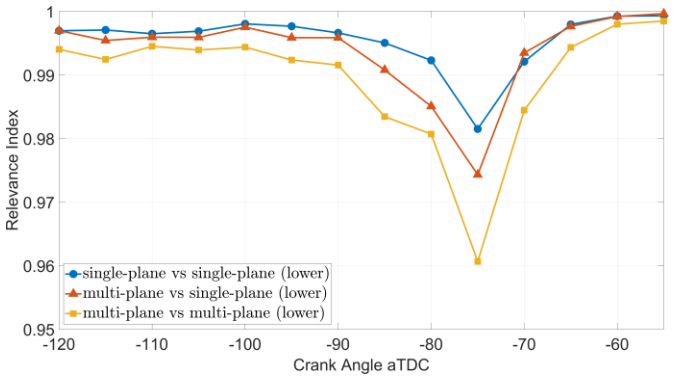

Figure 17 Relevance Index (RI) comparisons of the similarity of 250-cycle mean vector fields from the multi-plane and single-plane PIV techniques as a function of crank angle during the compression stroke for the lower plane. The 250-cycle datasets used for this comparison were obtained by splitting each of the 500-cycle multi-plane and single-plane datasets into two.

Rejected vectors

For the 15 mm plane separation of this work, cross-talk contributions from the out-of-focus plane do not bias the derived velocity fields in a way that changes the mean flow field beyond that which can be attributed to cyclic variability.

An alternative mechanism by which cross-talk could disturb the measurement without perturbing the mean flow field is by biasing the correlation map generated during PIV vector calculation such that the correlation peak does not satisfy the vector validation routines, leading to a rejected vector at that location and timing.

The number of rejected vectors is less than 1% for the majority of the locations within both the multi-plane and single-plane PIV mean flow fields, averaged across all measurement timings (−120°CA aTDC to −55°CA aTDC) [Figure 18].

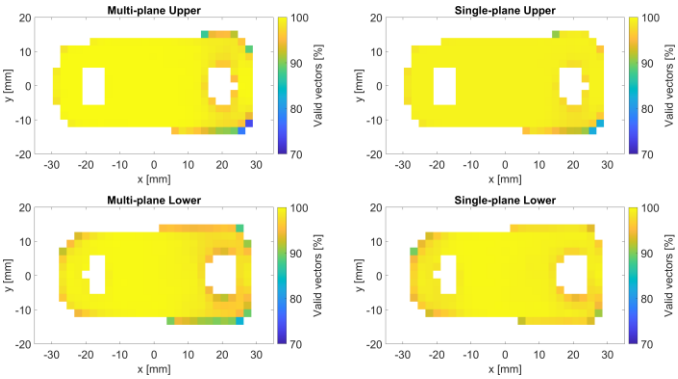

Figure 18 Percentage of valid vectors at each location contributing to the mean velocity field, averaged over all measurement timings (−120°CA to −55°CA aTDC).

Conclusions

Simultaneous multi-plane PIV measurements on two parallel, offset planes have been performed within a motored optically accessible spark ignition engine using a single-camera 2D2C PIV system. The imaging setup leverages a narrow depth of field and, similarly to a z-splitter arrangement for multifocal plane microscopy, is modified with variable optical path length image splitting optics to image two planes at different depths onto a single camera sensor. The degree of defocus of the droplet images from the out-of-focus plane reduces their contributions to the cross-correlation of the PIV processing routine, ensuring that the resulting vectors represent the motion of droplet images from only the in-focus plane. This defocus approach to multi-plane PIV plane discrimination was validated using static representative PIV targets and for plane separations 15 mm and greater achieved: an average error of ≤0.6%, a standard deviation of <1.5% and individual derived velocities all within 6% of the correct value.

500-cycle mean in-cylinder velocity fields obtained via simultaneous multi-plane PIV were compared to those obtained via sequential conventional single-plane PIV measurements. Motion of the tumble vortex centre during the compression stroke enabled investigation of three distinct flow conditions across the two parallel horizontal swirl planes: a) similar flows with slight differences in direction and magnitude, b) one stable, high velocity flow and one highly variable flow with regions of low velocity and c) opposed flows. Across the three flow conditions, a spatially-averaged difference of 0.23 ± 0.26 ms^{-1} (95% CI) between the multi-plane PIV and single-plane PIV mean fields was obtained for mean velocities spanning $0 – 10$ ms^{-1}. This difference encompasses both uncertainty in the multi-plane and single-plane PIV techniques and the influence of cyclic variability of the in-cylinder flow. The number of missing vectors as a result of failing the vector validation steps during the PIV processing was less than 1% for the majority of the locations within both the multi-plane and single-plane PIV mean flow fields.

Quantitative comparisons of the single-plane PIV to multi-plane PIV data via the Relevance Index (RI) produced RI values above 0.97 for all measurement timings during the compression stroke. Additionally, comparisons of sequential sets of 250-cycle mean single-plane PIV velocity fields, in order to approximate the best achievable RI values due to cyclic variability of the in-cylinder flow, produced RI values of 0.98 and above. Larger datasets in future work will reduce the influence of cyclic variability and may enable the inherent increase in uncertainty of the multi-plane PIV technique over standard single-plane PIV to be quantified.

The multi-plane PIV via depth-of-field technique may be extended to more than two planes with suitable image splitting optics or additional cameras and is compatible with conventional methods for distinguishing PIV planes, such as wavelength and polarization, further increasing the number of potential planes for simultaneous multi-plane PIV measurements.

Funding

This research was funded in whole or in part by an Engineering and Physical Sciences Research Council Prosperity Partnership, grant number EP/T005327/1. For the purpose of Open Access, the authors have applied a CC BY 4.0 public copyright licence to any Author Accepted Manuscript (AAM) version arising from this submission. The final version of record is published on SAE Mobilus® at https://doi.org/10.4271/2023-01-0213.

Acknowledgements

The Prosperity Partnership is a collaboration between Jaguar Land Rover, Siemens Digital Industries Software, the University of Bath and the University of Oxford. The authors would also like to thank

the Department of Engineering Science technicians and maintenance teams for facilities support.

Data availability

Due to confidentiality agreements with research collaborators, data supporting this paper can only be made available to *bona fide* researchers subject to a non-disclosure agreement. Details of the data and how to request access are available from the "Oxford Research Archive" repository at https://ora.ox.ac.uk/.

Contact Information

Christopher Willman
Department of Engineering Science, Parks Road, OX1 3PJ
christopher.willman@eng.ox.ac.uk

Definitions/Abbreviations

2D2C	Two-dimensional, two-component
aTDC	After Top-Dead-Centre (firing)
°CA	Crank Angle Degrees
CI	Confidence Interval
GDI	Gasoline Direct Injection
GDPT	General Defocusing Particle Tracking
ICE	Internal Combustion Engine
PIV	Particle Image Velocimetry
μPIV	Microscopic Particle Image Velocimetry
RI	Relevance Index

References

[1] A. K. Agarwal, S. Gadekar, and A. P. Singh, "In-cylinder air-flow characteristics of different intake port geometries using tomographic PIV," *Phys. Fluids*, vol. 29, no. 9, 2017, doi: 10.1063/1.5000725.

[2] M. Braun, W. Schröder, and M. Klaas, "High-speed tomographic PIV measurements in a DISI engine," *Exp. Fluids*, vol. 60, p. 146, 2019, doi: 10.1007/s00348-019-2792-4.

[3] D. Schanz, S. Gesemann, and A. Schröder, "Shake-The-Box: Lagrangian particle tracking at high particle image densities," *Exp. Fluids*, vol. 57, no. 5, pp. 1–27, 2016, doi: 10.1007/s00348-016-2157-1.

[4] M. P. Wernet, "Comparison of Tomo-PIV Versus Dual Plane PIV on a Synthetic Jet Flow," *Nasa*, no. May 2017, p. 219508, 2017.

[5] M. Raffel, C. E. Willert, F. Scarano, C. Kähler, S. T. Wereley, and J. Kompenhans, *Particle Image Velocimetry: A Practical Guide*, 3rd ed. Springer International Publishing, 2018.

[6] J. A. Mullin and W. J. A. Dahm, "Dual-plane stereo particle image velocimetry measurements of velocity gradient tensor fields in turbulent shear flow. I. Accuracy assessments," *Phys. Fluids*, vol. 18, no. 3, 2006, doi: 10.1063/1.2166447.

[7] J. Bode, J. Schorr, C. Krüger, A. Dreizler, and B. Böhm, "Influence of three-dimensional in-cylinder flows on cycle-to-cycle variations in a fired stratified DISI engine measured by time-resolved dual-plane PIV," *Proc. Combust. Inst.*, vol. 36, no. 3, pp. 3477–3485, 2017, doi: 10.1016/j.proci.2016.07.106.

[8] B. Ganapathisubramani, E. K. Longmire, I. Marusic, and S. Pothos, "Dual-plane PIV technique to determine the complete velocity gradient tensor in a turbulent boundary layer," *Exp. Fluids*, vol. 39, no. 2, pp. 222–231, 2005, doi: 10.1007/s00348-005-1019-z.

[9] M. Shimura, T. Ueda, G. M. Choi, M. Tanahashi, and T. Miyauchi, "Simultaneous dual-plane CH PLIF, single-plane OH PLIF and dual-plane stereoscopic PIV measurements in methane-air turbulent premixed flames," *Proc. Combust. Inst.*, vol. 33, no. 1, pp. 775–782, 2011, doi: 10.1016/j.proci.2010.05.026.

[10] J. Kerl, C. Lawn, and F. Beyrau, "Three-dimensional flame displacement speed and flame front curvature measurements using quad-plane PIV," *Combust. Flame*, vol. 160, no. 12, pp. 2757–2769, 2013, doi: 10.1016/j.combustflame.2013.07.002.

[11] Y. Naka, K. Tomita, M. Shimura, N. Fukushima, M. Tanahashi, and T. Miyauchi, "Quad-plane stereoscopic PIV for fine-scale structure measurements in turbulence," *Exp. Fluids*, vol. 57, no. 5, pp. 1–20, 2016, doi: 10.1007/s00348-016-2146-4.

[12] J. Bode, J. Schorr, C. Krüger, A. Dreizler, and B. Böhm, "Influence of the in-cylinder flow on cycle-to-cycle variations in lean combustion DISI engines measured by high-speed scanning-PIV," *Proc. Combust. Inst.*, vol. 37, no. 4, 2019, doi: 10.1016/j.proci.2018.07.021.

[13] W. Zhou, Y. Zhang, B. Chen, C. Tropea, R. Xu, and X. Cai, "Sensitivity analysis and measurement uncertainties of a two-camera depth from defocus imaging system," *Exp. Fluids*, vol. 62, no. 11, pp. 1–14, 2021, doi: 10.1007/s00348-021-03316-2.

[14] W. Zhou, C. Tropea, B. Chen, Y. Zhang, X. Luo, and X. Cai, "Spray drop measurements using depth from defocus," *Meas. Sci. Technol.*, vol. 31, no. 7, 2020, doi: 10.1088/1361-6501/ab79c6.

[15] R. Barnkob and M. Rossi, "General defocusing particle tracking: fundamentals and uncertainty assessment," *Exp. Fluids*, vol. 61, no. 4, pp. 1–14, 2020, doi: 10.1007/s00348-020-2937-5.

[16] M. Rossi and R. Barnkob, "A fast and robust algorithm for

general defocusing particle tracking," *Meas. Sci. Technol.*, vol. 32, no. 1, 2021, doi: 10.1088/1361-6501/abad71.

[17] C. E. Willert and M. Gharib, "Three-dimensional particle imaging with a single camera," *Exp. Fluids*, vol. 12, no. 6, pp. 353–358, 1992, doi: 10.1007/BF00193880.

[18] L. Kajitani and D. Dabiri, "A full three-dimensional characterization of defocusing digital particle image velocimetry," *Meas. Sci. Technol.*, vol. 16, no. 3, pp. 790–804, 2005, doi: 10.1088/0957-0233/16/3/022.

[19] L. Kajitani and D. Dabiri, "A full three-dimensional characterization of defocusing digital particle image velocimetry (Measurement Science and Technology (2005) 16 (790-804))," *Meas. Sci. Technol.*, vol. 19, no. 4, pp. 9–11, 2008, doi: 10.1088/0957-0233/19/4/049801.

[20] F. Pereira, M. Gharib, D. Dabiri, and D. Modarress, "Defocusing digital particle image velocimetry: A 3-component 3-dimensional DPIV measurement technique. Application to bubbly flows," *Exp. Fluids*, vol. 29, no. SUPPL. 1, 2000, doi: 10.1007/s003480070010.

[21] C. Cierpka, M. Rossi, R. Segura, F. Mastrangelo, and C. J. Kähler, "A comparative analysis of the uncertainty of astigmatism-μPTV, stereo-μPIV, and μpIV," *Exp. Fluids*, vol. 52, no. 3, pp. 605–615, 2012, doi: 10.1007/s00348-011-1075-5.

[22] C. Cierpka, R. Segura, R. Hain, and C. J. Kähler, "A simple single camera 3C3D velocity measurement technique without errors due to depth of correlation and spatial averaging for microfluidics," *Meas. Sci. Technol.*, vol. 21, no. 4, 2010, doi: 10.1088/0957-0233/21/4/045401.

[23] P. A. Dalgarno *et al.*, "Multiplane imaging and three dimensional nanoscale particle tracking in biological microscopy," *Opt. Express*, vol. 18, no. 2, p. 877, 2010, doi: 10.1364/oe.18.000877.

[24] S. Abrahamsson *et al.*, "MultiFocus Polarization Microscope (MF-PolScope) for 3D polarization imaging of up to 25 focal planes simultaneously," *Opt. Express*, vol. 23, no. 6, p. 7734, 2015, doi: 10.1364/oe.23.007734.

[25] S. Ram, P. Prabhat, J. Chao, E. S. Ward, and R. J. Ober, "High accuracy 3D quantum dot tracking with multifocal plane microscopy for the study of fast intracellular dynamics in live cells," *Biophys. J.*, vol. 95, no. 12, pp. 6025–6043, 2008, doi: 10.1529/biophysj.108.140392.

[26] P. Prabhat, S. Ram, E. Sally Ward, and R. J. Ober, "Simultaneous imaging of different focal planes in fluorescence microscopy for the study of cellular dynamics in three dimensions," *IEEE Trans. Nanobioscience*, vol. 3, no. 4, pp. 237–242, 2004, doi: 10.1109/TNB.2004.837899.

[27] S. Xiao, H. Gritton, H.-A. Tseng, D. Zemel, X. Han, and J. Mertz, "High-contrast multifocus microscopy with a single camera and z-splitter prism," *Optica*, vol. 7, no. 11, p. 1477, 2020, doi: 10.1364/optica.404678.

[28] M. Rossi, R. Segura, C. Cierpka, and C. J. Kähler, "On the effect of particle image intensity and image preprocessing on the depth of correlation in micro-PIV," *Exp. Fluids*, vol. 52, no. 4, pp. 1063–1075, 2012, doi: 10.1007/s00348-011-1194-z.

[29] A. Liberzon, R. Gurka, and G. Hetsroni, "XPIV-Multi-plane stereoscopic particle image velocimetry," *Exp. Fluids*, vol. 36, no. 2, pp. 355–362, 2004, doi: 10.1007/s00348-003-0731-9.

[30] W. Thielicke and R. Sonntag, "Particle Image Velocimetry for MATLAB: Accuracy and enhanced algorithms in PIVlab," *J. Open Res. Softw.*, vol. 9, pp. 1–14, 2021, doi: 10.5334/JORS.334.

[31] L. Shen, C. Willman, R. Stone, T. Lockyer, R. Magnanon, and G. Virelli, "Multi-Plane PIV Measurements in a Gasoline Direct Injection Engine," *SAE Int. J. Adv. & Curr. Prac. in Mobility* 3(1):223-239, 2021, doi: 10.4271/2020-01-2049.

[32] K. Liu and D. C. Haworth, "Development and Assessment of POD for Analysis of Turbulent Flow in Piston Engines," 2011, doi: 10.4271/2011-01-0830.

[33] Y. Wang, D. L. S. Hung, H. Zhuang, and M. Xu, "Cycle-to-Cycle Analysis of Swirl Flow Fields inside a Spark- Ignition Direct-Injection Engine Cylinder Using High-Speed Time-Resolved Particle Image Velocimetry," 2016, doi: 10.4271/2016-01-0637.